3-2009

Substrate Binding Preferences and pK_a Determinations of a Nitrile Hydratase Model Complex: Variable Solvent Coordination to [(bmmp-TASN)Fe]OTf

Martin G. O'Toole
University of Louisville

Brian Bennett
Marquette University, brian.bennett@marquette.edu

Mark S. Mashuta
University of Louisville

Craig A. Grapperhaus
University of Louisville

Inorganic Chemistry, Vol. 48, No. 5 (2 March 2009): 2300-2308. DOI.

Substrate Binding Preferences and pK_a Determinations of a Nitrile Hydratase Model Complex: Variable Solvent Coordination to [(bmmp-TASN)Fe]OTf

Martin G. O'Toole
Department of Chemistry, University of Louisville, Louisville, Kentucky
Brian Bennett
National Biomedical EPR Center, Department of Biophysics, Medical College of Wisconsin, Milwaukee, Wisconsin
Mark S. Mashuta
Department of Chemistry, University of Louisville, Louisville, Kentucky
Craig A. Grapperhaus
Department of Chemistry, University of Louisville, Louisville, Kentucky

SUBJECTS:
Iron, Ligands, Nitrogen compounds

Abstract

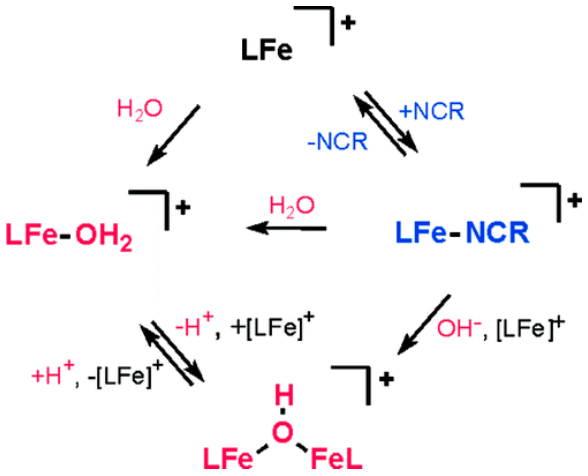

The five-coordinate iron-dithiolate complex (*N*,*N*'-4,7-bis-(2'-methyl-2'-mercatopropyl)-1-thia-4,7-diazacyclononane)iron(III), **[LFe]**$^+$, has been isolated as the triflate salt from reaction of the previously reported **LFeCl** with thallium triflate. Spectroscopic characterization confirms an S = 1/2 ground state in non-coordinating solvents with room temperature μ_{eff} = 1.78 μ_B and electron paramagnetic resonance (EPR) derived g-values of g_1 = 2.04, g_2 = 2.02 and g_3 = 2.01. **[LFe]**$^+$ binds a variety of coordinating solvents resulting in six-coordinate complexes **[LFe-solvent]**$^+$. In acetonitrile the low-spin **[LFe-NCMe]**$^+$ (g_1 = 2.27, g_2 = 2.18, and g_3 = 1.98) is in equilibrium with **[LFe]**$^+$ with a binding constant of K_{eq} = 4.7 at room temperature. Binding of H_2O, DMF, methanol, DMSO, and pyridine to **[LFe]**$^+$ yields high-spin six-coordinate complexes with EPR spectra that display significant strain in the rhombic zero-field splitting term E/D. Addition of 1 equiv of triflic acid to the previously reported diiron species **$(LFe)_2O$** results in the formation of **$[(LFe)_2OH]OTf$**, which has been characterized by X-ray crystallography. The aqueous chemistry of **[LFe]**$^+$ reveals three distinct species as a function of pH: **$[LFe\text{-}OH_2]^+$**, **$[(LFe)_2OH]OTf$**, and **$(LFe)_2O$**. The pK_a values for **$[LFe\text{-}OH_2]^+$** and **$[(LFe)_2OH]OTf$** are 5.4 ± 0.1 and 6.52 ± 0.05, respectively.

Synopsis

A five coordinate iron-dithiolate model complex of nitrile hydratase, [(bmmp-TASN)Fe]$^+$, **[LFe]**$^+$ has been synthesized and shown to bind both substrates relevant to enzymatic hydrolysis (water and nitriles). **[LFe]**$^+$ binds nitriles reversibly but shows a strong preference for water-binding. In water, **[LFe]**$^+$ yields three isolable species as a function of pH: **$[LFe\text{-}OH_2]^+$**, **$[(LFe)_2OH]^+$**, and **$(LFe)_2O$**.

Introduction

Small molecule model complexes of the non-heme iron enzyme nitrile hydratase (NHase) have been instrumental in elucidating the geometric and electronic structure of the enzyme active site.(1-11) NHase, which catalyzes the hydrolysis of nitriles to amides, possesses either a low-spin Fe(III) or non-corronid Co(III) in an unusual nitrogen/sulfur-rich environment with a primary coordination sphere consisting of two deprotonated amides from the peptide backbone, three cysteine derived sulfur donors (now known to exist in three different oxidation states), and a variable coordination site for interacting with substrates/products, Figure 1.(12-18) On the basis of spectroscopic and computational results, several catalytic mechanisms have been proposed.(4, 8, 19-21) Despite intensive efforts, it is still uncertain whether water, nitrile, or both substrates coordinate at the active site during catalysis.

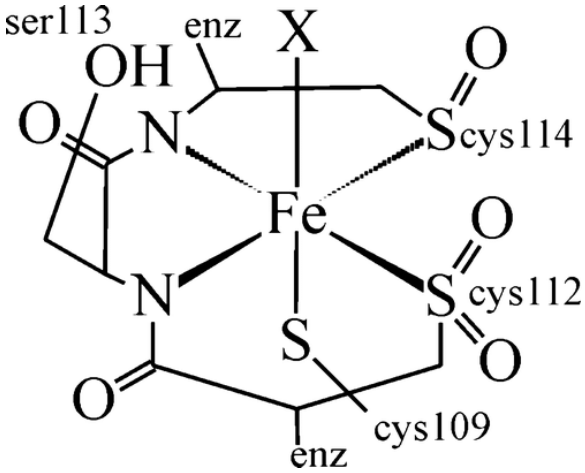

Figure 1. Representation of the active site of nitrile hydratase.

The substrate binding affinities of active site models have not provided consistent results.(22, 23) A high-spin (*S* = 5/2), five-coordinate iron complex with deprotonated amides and thiolate donors coordinates water but shows no affinity for nitriles.(22) A closely related low-spin (*S* = 1/2), five-coordinate iron complex featuring imine nitrogen donors and thiolates exclusively binds nitriles at low temperature but undergoes ligand degradation upon exposure to water.(23) To our knowledge, a single model complex that coordinates both nitrile and water has not yet been reported. In this manuscript we report the five-coordinate iron dithiolate, *N*,*N*′-bis-(2′-methyl-2′-mercaptopropyl)-1-thia-4,7-diazacyclononane)iron(III) triflate (**[LFe]OTf**). **[LFe]OTf** binds water, nitriles, and amides allowing for the first time a direct comparison of substrate (and product) binding affinities in a single model complex. Additionally, the pK_a of the water and hydroxide bound derivatives of **[LFe]OTf** have been evaluated and offer insight regarding the need for low-spin iron at the enzyme active site.

Experimental Section

Materials and Methods

All reagents were obtained from commercially available sources and used as received unless otherwise noted. All solvents were dried and freshly distilled using standard techniques under a nitrogen atmosphere and degassed using freeze−pump−thaw techniques.(24, 25) All reactions were conducted using standard Schlenk techniques under an argon atmosphere or in an argon-filled glovebox unless otherwise noted.(26) The complexes [(bmmp-TASN)FeCl], **LFeCl**, and [(bmmp-TASN)Fe]$_2$O, **(LFe)$_2$O**, were prepared as previously reported.(2) Thallium triflate was prepared from thallium carbonate and triflic acid according to published protocols.(27)

N,*N*′-Bis-(2′-methyl-2′-mercaptopropyl)-1-thia-4,7-diazacyclononane iron(III) Triflate ([LFe]OTf·0.5CH$_2$Cl$_2$)

To a suspension of 100 mg (0.24 mmol) of LFeCl in 100 mL of dry acetonitrile was added dropwise via cannula a solution of 86 mg (0.24 mmol) of thallium triflate in 15 mL of acetonitrile. After stirring for 15 h, the solvent was removed under vacuum, and the product extracted into 60 mL of dichloromethane followed by filtration through a fritted tube. Removal of solvent from the filtrate yielded [LFe]OTf·0.5CH$_2$Cl$_2$ as a dark blue solid. Yield: 81 mg (0.15 mmol, 63%). Electronic absorption (dichloromethane (22 °C)): λ_{max}(ε): 274(7601), 317(6740), 427(2570), 504(1400), 623(1600). IR (KBr pellet), cm^{-1}: 3436 (br), 2949 (m), 2912 (m), 2880 (m), 2843 (m), 1450 (m), 1262 (s), 1135 (m), 1102 (m), 1074 (m), 1029 (s), 804 (m), 636 (m). MS-ESI, *m*/*z* calcd. For $C_{14}H_{28}N_2S_3Fe$, [M+]

376.08; Found, 376.05. Anal. Calcd. for $C_{15.5}H_{31}N_2S_4O_3F_3FeCl$([LFe]OTf·0.5$CH_2Cl_2$): C, 31.48; H, 4.95; N, 4.59. Found: C, 31.17; H, 4.92; N, 4.88.

[(LFe)$_2$OH]Tf

A solution of **(LFe)$_2$O** (50 mg, 65 μmol) in 100 mL of acetonitrile was cooled to −15 °C in a dry ice/ethylene glycol bath. A solution of 5.7 μL (9.7 mg, 65 μmol) of 98% triflic acid in 10 mL of acetonitrile was added dropwise via cannula over a 30 min. period. The solution was stirred for 2 h as it gradually warmed to room temperature. The solution was filtered through a fritted tube and concentrated to 15 mL. Diethyl ether addition led to precipitation of **[(LFe)$_2$OH]Tf** as a purple solid. Yield: 45 mg (49 μmol, 75%). X-ray quality crystals were obtained by vapor diffusion of diethyl ether into a methanol solution of **2** at 4 °C under an argon atmosphere. Electronic absorption (acetonitrile) λ_{max}(ε): 311(3600), 433(700), 602(1600). IR (KBr pellet), cm^{-1}: 3490 (br), 2958 (m), 2913 (m), 2880 (m), 2847 (m), 1454 (m), 1254 (s), 1147 (m), 1131 (m), 1074 (m), 1029 (s), 976 (m), 641 (s), 518 (m). Anal. Calcd for $C_{29}H_{58}N_4S_8O_7F_6Fe_2$(**[(LFe)$_2$OH]OTf·HOTf**): C, 36.24; H, 5.88; N, 5.64. Found: C, 36.92; H, 5.77; N, 5.57.

Physical Methods

Elemental analyses were obtained from Midwest Microlab (Indianapolis, IN). Infrared spectra were recorded on a Thermo Nicolet Avatar 360 spectrometer at 4 cm^{-1} resolution. ^{1}H NMR spectra were obtained on a Varian Inova500 500 MHz spectrometer. Mass spectrometry (ESI-MS) was performed by the Laboratory for Biological Mass Spectrometry at Texas A&M University. The room temperature magnetic moment of **[LFe]OTf** was determined by the Evan's method in dichloromethane with use of residual CH_2Cl_2 peak, and its shifted counterpart in calculation of μ_{eff}.(28) Cyclic voltammetry (CV) was performed using a PAR 273 potentiostat with a three electrode cell (glassy carbon working electrode, platinum wire counter electrode, and a Ag/AgCl pseudo reference electrode) at room temperature in an argon filled glovebox. All potentials were scaled to a ferrocene/ferrocenium standard using an internal reference. Catalytic trials (see Supporting Information) were monitored by gas chromatography using an HP 5890 series II chromatograph fitted with a flame ionization detector using compressed air as a carrier gas with an RTX-1 column (60 m length, i.d. 32, serial number 469083) from Restek Corporation.

Electronic absorption spectra were recorded with an Agilent 8453 diode array spectrometer with air free 1 cm path length quartz cell or in a custom-made Dewar flask with a 1 cm path length quartz sample compartment. The equilibrium constant for acetonitrile binding was determined as described in the Supporting Information based on minimization of the R^2 value of the resulting van't Hoff plot using previously reported methods:(23, 29) The pK_a values for **[LFe-OH$_2$]$^+$** and **[(LFe)$_2$OH]OTf** were determined spectrophotometrically in a 70:30 water/acetone mixture because of poor solubility of **(LFe)$_2$O** in aqueous solution(30) using a Corning pH 440 m with full details in the Supporting Information.

X-band electron paramagnetic resonance (EPR) spectra were obtained either on a Bruker EMX EPR spectrometer (77 K, 6.3 mW, modulation amplitude 5 G) or on a Bruker EleXsys E600 spectrometer (20 K, 2 mW, modulation amplitude 10 G) equipped with an ER4116DM TE_{012}/TE_{102} dual-mode cavity and an Oxford Instruments ESR900 helium flow cavity. The S = 1/2 spectra were modeled using SIMPOW.(31) Computer simulations of S = 5/2 spectra were carried out using matrix diagonalization with XSophe v.1.1.3,(32) assuming a spin Hamiltonian $\boldsymbol{H}$ = β**g.B.S** + **S.D.S** and including distributions ("strains") in the zero-field splitting parameters, σD and σE/D.

Crystallographic Studies

A dark purple trapezoidal prism 0.29 × 0.22 × 0.05 mm^3 crystal of **[(LFe)$_2$OH]OTf** was selected for X-ray data collection on a Bruker SMART APEX CCD diffractometer. Frame data were collected (SMART(33) v5.632) and processed (SAINT(34) v6.45a) to determine final unit cell parameters: a = 15.472(6) Å, b = 10.629(4) Å, c = 25.894(13) Å, β = 95.172(5)°, V = 4241(3) Å^3, Z = 4, and ρ_{calcd} = 1.477 Mg m^{-3}. The raw *hkl* data were corrected for

absorption (SADABS(35) v2.10; transmission min./max. = 0.744/0.948; μ = 1.082 mm^{-1}) and the structure was solved by Patterson methods (SHELXTL(36-38) (v 6.14) suite of programs) in the space group *Ia*. For all 9283 unique reflections (*R*(int) = 0.0273) the final anisotropic full matrix least-squares refinement on F^2 for 468 variables converged at R1 = 0.0420 and wR2 = 0.0994 with a GOF of 1.08. Crystallographic parameters for **[(LFe)$_2$OH]OTf** are displayed in Table 1 with additional experimental details provided in the Supporting Information.

Table 1. Crystal Data and Structure Refinement for [(LFe)$_2$OH]OTf

identification code	**[(LFe)$_2$OH]OTf**
empirical formula	$C_{29}H_{57}F_3Fe_2N_4O_4\ S_7 \cdot 0.75(CH_3OH)$
formula weight	942.94
temperature	100(2) K
wavelength	0.71073 Å
crystal system	monoclinic
space group	*Ia*
unit cell dimensions	*a* = 15.472(6) Å
	b = 10.629(4) Å
	c = 25.894(13) Å
	β = 95.172(5)°.
volume	4241(3) $Å^3$
Z	4
density (calculated)	1.477 Mg/m^3
absorption coefficient	1.082 mm^{-1}
F(000)	1982
crystal size	0.29 × 0.22 × 0.05 mm^3
theta range for data collection	2.64 to 28.14°
crystal color, habit	dark purple trapezoidal prism
index ranges	−20 ≤ *h* ≤ 20
	−14 ≤ *k* ≤ 13
	−33 ≤ *l* ≤ 33
reflections collected	18021
independent reflections	9283 [*R*(int) = 0.0273]
completeness to theta = 28.14°	95.7%
absorption correction	SADABS
max. and min. transmission	0.948 and 0.744
refinement method	full-matrix least-squares on F^2
data/restraints/parameters	9283/4/468
goodness-of-fit on F^2	1.08
final *R* indices [*I* > 2sigma(*I*)]	R1 = 0.0388, wR2 = 0.0965
R indices (all data)	R1 = 0.0420, wR2 = 0.0994
absolute structure parameter	0.030(12)
largest diff. peak and hole	1.092 and −0.326 e $Å^{-3}$

Results and Discussion

Synthesis and Characterization

Previously we reported **LFeCl** (L = bmmp-TASN) as a model complex of nitrile hydratase.(2) The coordinated chloride was not displaced by water or nitrile, although under basic conditions the μ-oxo complex **$(LFe)_2O$** was obtained. Herein we report metathesis of the chloride with thallium triflate to yield the five-coordinate complex **[LFe]OTf**, Scheme 1. The infrared spectrum of **[LFe]OTf** displays strong absorptions at 1262 and 1029 cm^{-1} attributed to the triflate counterion but is otherwise similar to that of **LFeCl**. The room temperature magnetic moment of **[LFe]OTf** in dichloromethane (1.78 μ_B) is consistent with the spin-only value for low-spin iron(III). Mass spectral analysis of **[LFe]OTf** from dichloromethane, acetonitrile, or aqueous solutions displays a major peak at *m/z* = 376.08 as expected for **$[LFe]^+$** with no evidence of triflate or solvent coordination in the gas phase.

Scheme 1

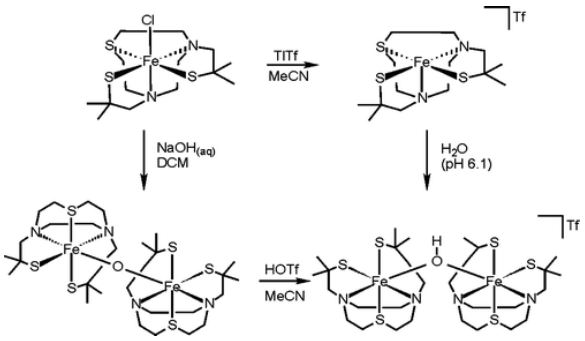

As a solid **[LFe]OTf** is vivid blue; however, in solution the color depends on equilibrium solvent binding. In water, three species (**$[LFe\text{-}OH_2]^+$**, **$[(LFe)_2OH]^+$**, and **$(LFe)_2O$**) were observed as a function of pH. [**$(LFe)_2OH$]OTf** is also obtained by stoichiometric addition of triflic acid to acetontrile solutions of **$(LFe)_2O$** with a corresponding bathochromic shift in the low energy absorption band from 553 to 603 nm, Figure 2. The infrared spectrum of **$[(LFe)_2OH]$OTf** is marked by bands at 1254 and 1029 cm^{-1} because of the triflate counterion. Also of note is the absence of the Fe−O−Fe stretch at 800 cm^{-1} found in the IR spectrum of the precursor μ-oxo complex.(2) The **$[(LFe)_2OH]$OTf** complex is soluble in water, acetonitrile, alcohols, and sparingly soluble in dichloromethane, yielding violet colored solutions in each case.

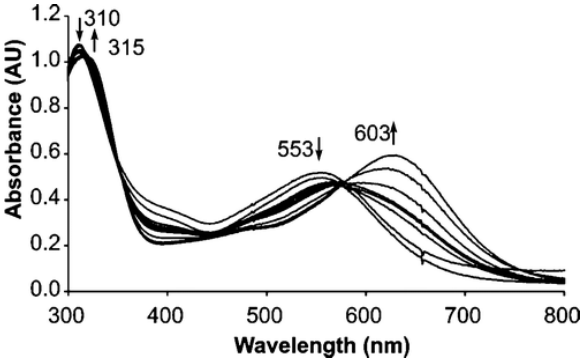

Figure 2. UV/visible spectra during the synthesis of **$[(LFe)_2OH]$OTf** (3 mM) in acetonitrile.

Structural Characterization of $[(LFe)_2OH]$OTf

The complex [**$(LFe)_2OH$]OTf** crystallizes in the monoclinic space group *Ia* with one metal containing cation, [**$(LFe)_2OH]^+$**, one triflate anion, and a partial occupancy methanol solvent molecule. The position of the hydrogen

atom of the bridging hydroxide was determined from an electron density map and refined isotropically. An Oak Ridge Thermal Ellipsoid Plot (ORTEP)(39) representation of $[\mathbf{(LFe)_2OH}]^+$ is presented in Figure 3 with selected bond distances and angles given in Table 2. As with all other complexes of **L**, the TASN ligand backbone constrains the two amines and thioether sulfur to a facial coordination mode.(1, 2, 11) For each iron center, the three sulfur donors are meridional with each sulfur cis to the hydroxide bridge. An amine nitrogen occupies the position trans to the bridging hydroxide. The iron-ligand bond distances of $\mathbf{[(LFe)_2OH]}^+$ are within the ranges expected for high spin Fe(III).(2, 11, 40)

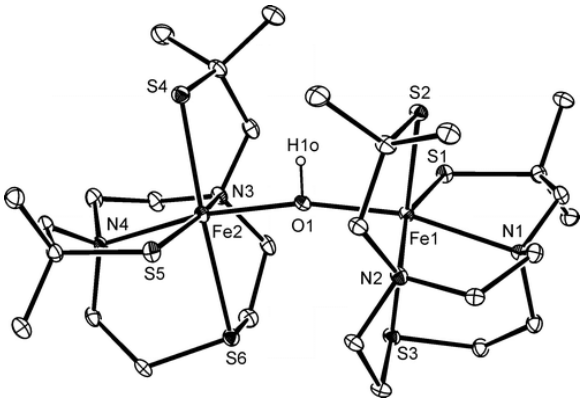

Figure 3. ORTEP view of $\mathbf{[(LFe)_2OH]}^+$ showing 30% probability displacement ellipsoids. Calculated H atoms, solvent, and triflate counterion have been omitted.

Table 2. Selected Bond Distances (Å) and Bond Angles (deg) for $[(LFe)_2OH]OTf$

Fe1−S1	2.3004(12)	Fe1−N1	2.263(3)
Fe1−S2	2.3262(13)	Fe1−N2	2.242(3)
Fe1−S3	2.5385(14)	Fe1−O1	2.002(3)
Fe2−S4	2.3250(12)	Fe2−N3	2.244(3)
Fe2−S5	2.2961(12)	Fe2−N4	2.258(3)
Fe2−S6	2.5565(13)	Fe2−O1	1.998(3)
		$O1-H1_o$	0.841(19)
N1−Fe1−N2	79.10(11)	N1−Fe1−S1	83.56(8)
N2−Fe1−S2	84.11(8)	N1−Fe1−S2	96.11(8)
N2−Fe1−S3	80.71(8)	S1−Fe1−S2	102.22(4)
O1−Fe1−S2	93.91(8)	Fe1−O1−Fe2	166.71(14)
N3−Fe2−N4	78.86(11)	N3−Fe2−S4	84.26(9)
N3−Fe2−S6	81.10(8)	N4−Fe2−S5	83.95(8)
N4−Fe2−S6	80.96(8)	S4−Fe2−S5	100.95(4)
$Fe1-O1-H1_0$	96(3)	$Fe2-O1-H1_0$	98(3)

Comparison of the structure of $[\mathbf{(LFe)_2OH]OTf}$ with previously reported crystallographic data for the related μ-oxo complex, $\mathbf{(LFe)_2O}$, reveals important distinctions between the two structures.(2) The Fe−O−Fe angle for $\mathbf{[(LFe)_2OH]}^+$ is 166.71(14)°, while the corresponding angle for $\mathbf{(LFe)_2O}$ is 180.0°. This decrease in Fe−O−Fe bond angle results from protonation of the bridging oxo ligand.(41-43) The steric bulk of the ligands force a severe distortion of the idealized trigonal arrangement about the bridging oxygen atom, with Fe−O−H angles compressed to an average of 97°.

Solution Studies

The complex **[LFe]OTf** is soluble in a wide variety of polar and non-polar solvents yielding vivid green (5-coordinate) or blue (six-coordinate) solutions. A low energy charge transfer band near 600 nm, assigned as a thiolate to iron charge transfer, is observed for all six-coordinate complexes assigned as either **[LFe-solvent]**$^{+}$ or **LFe-OTf**, depending on reaction conditions.(44, 45) In contrast, the 5-coordinate complex, **[LFe]**$^{+}$ displays a lower energy band at 623 nm and a distinct shoulder at 427 nm.

Vacant Binding Site: Five-Coordinate, *S* = 1/2

Dichloromethane solutions of **[LFe]OTf** are green at all temperatures above −40 °C indicative of five-coordinate **[LFe]**$^{+}$. The room temperature UV−visible spectrum displays diagnostic bands at 315, 427, and 623 nm. Upon cooling to temperatures below −40 °C the color changes from green to blue because of triflate coordination. As shown in the Supporting Information, Figure S1, the low energy band shifts from 623 to 603 nm, and the shoulder at 427 nm decreases in intensity.

The lack of triflate coordination at room temperature is also evident in the cyclic voltammogram. In dichloromethane **[LFe]OTf** displays a pseudo-reversible event at −500 mV (vs Fc/Fc^{+}) assigned as $Fe^{III/II}$ and an irreversible oxidation at 510 mV assigned to the ligand, Supporting Information, Figure S2. The metal-based reduction potential is shifted by +560 mV with respect to **LFeCl** consistent with the loss of a donor atom. The oxidation is similarly shifted.

The EPR spectrum of **[LFe]OTf** in dichloromethane (77 K) indicates incomplete triflate coordination even at low temperature. The spectrum reveals a sharp signal for a low-spin component and a broad complex high-spin signal, Supporting Information, Figure S3, that gains intensity as the temperature is lowered, Supporting Information, Figure S4. The sharper signal attributable to **[LFe]**$^{+}$ was simulated (SIMPOW) with g-values of 2.06, 2.03, and 2.02, Figure 4.(31) This narrow g-value spread is atypical of low-spin iron(III)(46, 47) and more akin to that of metal-coordinated thiyl radicals, which show significantly less delocalization onto aromatic ligands than their phenoxyl counterparts.(48) Computational investigations by our group and others on low-spin iron(III)-thiolates show significant spin-density on sulfur (even in the absence of aromatic ligands) consistent with Fe(II)-thiyl radical character.(5, 11) The observed *S* = 1/2 ground state is consistent with increased Fe−S covalency as the thiolate compensates for the loss of the sixth donor and could result from coupling of either intermediate- or low-spin Fe(II) with the thiyl radical.(5, 11)

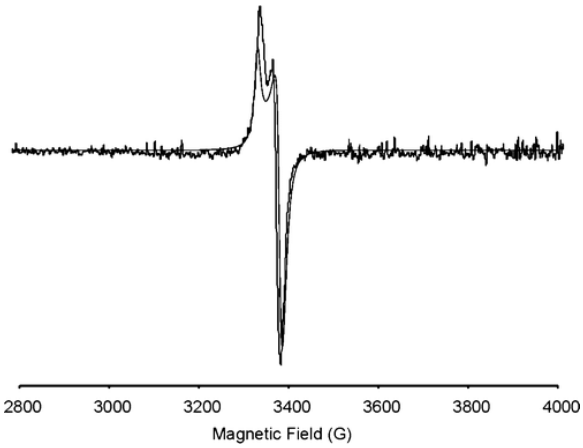

Figure 4. EPR spectrum (77 K) of **[LFe]OTf** in dichloromethane with simulation. Experimental parameters: microwave power = 6.3 mW, modulation amplitude = 5.35 G. Simulation parameters: g_1 = 2.06, g_2 = 2.03, g_3 = 2.02, W_1 = 21.80, W_2 = 39.87, W_3 = 21.23.

Nitrile Binding: Six-Coordinate, *S* = 1/2

The low affinity of **[LFe]**$^{+}$ for triflate ensures an accessible coordination site for solvent (substrate) binding. At 40 °C in acetonitrile, solutions of **[LFe]**$^{+}$ are green with absorbance bands at 315, 427, and 603 nm similar to the spectrum observed in dichloromethane and consistent with a five-coordinate complex. However, upon cooling to room temperature and below, the solution takes on a blue color as the peak at 427 nm loses intensity and the low energy band shifts toward 596 nm, Figure 5. The onset of these changes occurs at significantly higher temperature than in dichloromethane and arises because of nitrile coordination. The apparent equilibrium constants for nitrile binding of 4.7 at 298 K and 25 at −40 °C are similar to those reported by Kovacs in a related model complex.(23)

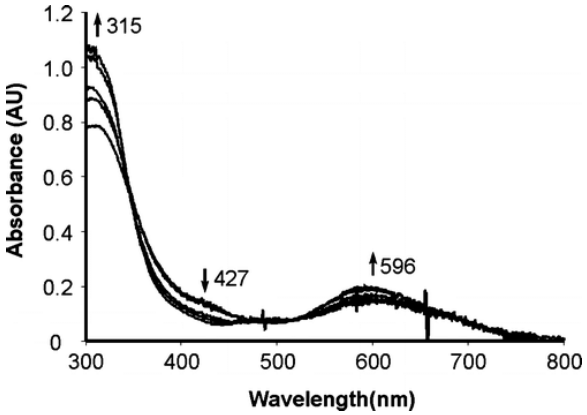

Figure 5. Variable temperature (40 to −43 °C) UV/visible spectra of **[LFe]OTf** (3 mM) in acetonitrile. Arrows denote changes in the spectra as the temperature is lowered.

The coordination of acetonitrile at room temperature is confirmed by CV. The CV of **[LFe]OTf** in acetonitrile, Supporting Information, Figure S2, displays a reversible event at −622 mV (vs Fc/Fc^{+}) assigned to the $Fe^{III/II}$ couple of **[LFe-NCMe]**$^{+}$and a chemically irreversible oxidation at 166 mV. The reduction potential is shifted by −120 mV as compared to that of **[LFe]**$^{+}$ consistent with the addition of a weakly coordinating ligand.

The EPR spectrum of **[LFe]OTf** (acetonitrile glass 77 K) also confirms equilibrium binding of acetonitrile, Figure 6A. In addition to the sharp axial signal of **[LFe]**$^{+}$ (g_1 = 2.04, g_2 = 2.02, g_3 = 2.01; 7% relative intensity), the spectrum also displays a rhombic signal (g_1 = 2.27, g_2 = 2.18, g_3 = 1.98; 93% relative intensity) attributed to **[LFe-NCMe]**$^{+}$. The large anisotropy in the g-values is typical of low-spin, six-coordinate Fe(III) complexes.(46, 47)

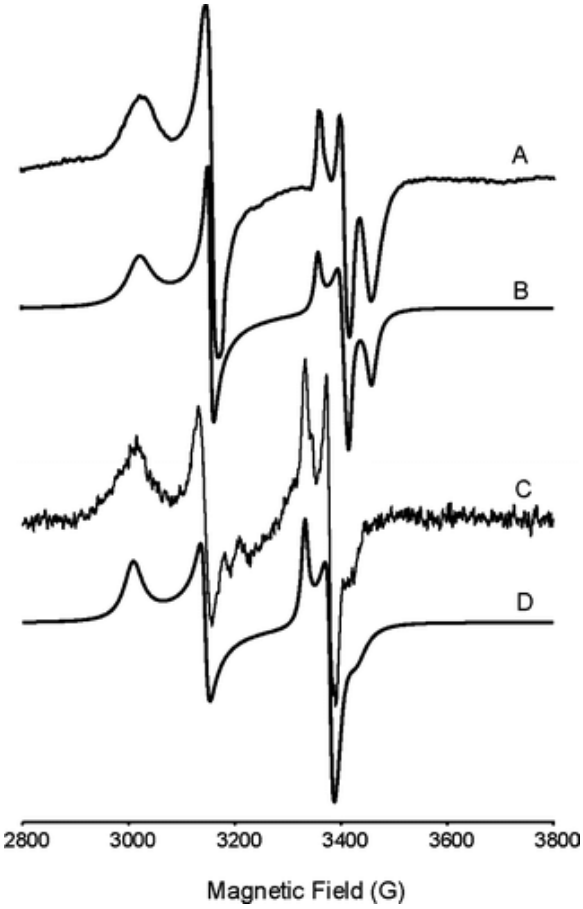

Figure 6. EPR spectra of **[LFe]OTf** in acetonitrile (A) with simulation (B) and **[LFe]OTf** in benzonitrile (C) with simulaton (D). Experimental parameters: (A) microwave power = 1.5 mW, modulation amplitude = 8.09 G; (C) microwave power = 1.99 mW, modulation amplitude = 6.00 G. Simulation parameters: (B) for **[LFe]**$^+$ g_1 = 2.01, g_2 = 2.02, g_3 = 2.02, W_1 = 19.40, W_2 = 25.80, W_3 = 28.15 and **[LFe-NCMe]**$^+$ g_1 = 2.27, g_2 = 2.18, g_3 = 1.98, W_1 = 17.95, W_2 = 91.21, W_3 = 33.17; (D) for **[LFe]**$^+$: g_1 = 2.06, g_2 = 2.03, g_3 = 2.03, W_1 = 21.73, W_2 = 40.05, W_3 = 21.08 and **[LFe-NCPh]**$^+$: g_1 = 2.28, g_2 = 2.18, g_3 = 2.00, W_1 = 64.78, W_2 = 26.50, W_3 = 46.33.

Similar results are obtained in benzonitrile, Figure 6B. A rhombic signal (g_1 = 2.28, g_2 = 2.18, g_3 = 2.00, relative intensity 85%) attributed to **[LFe-NCPh]**$^+$ is observed in addition to the axial signal of **[LFe]**$^+$. The similarity in *g*-values for the two nitrile bound derivatives **[LFe-NCMe]**$^+$and **[LFe-NCPh]**$^+$ implies that the identity of the nitrile donor does not significantly influence the electronic environment. This is consistent with recent computational studies that suggest the nitrile is not significantly polarized upon coordination to iron in NHase in contrast to expectations for a nitrile bound mechanism.(49)

Water and Other Donor Solvents: Six-Coordinate, *S* = 5/2

The donor ability of nitriles to **[LFe]**$^+$is limited, and low temperatures are required to facilitate coordination. Other solvents including water and DMF more strongly coordinate **[LFe]**$^+$ leading to high-spin derivatives. Solutions of **[LFe]**$^+$ in H_2O (pH < 6.1), DMF, DMSO, pyridine, or methanol are dark blue at all temperatures with a charge transfer band near 600 nm and no shoulder at 427 nm. The low energy band blue-shifts with increased σ-donor ability of the sixth ligand, although in H-donor solvents the shift is tempered by interactions between the solvent and sulfur, Supporting Information, Table S1.

The best evidence for solvent coordination is obtained from EPR spectroscopy. The complex EPR spectra of **[LFe]OTf** in DMSO, pyridine, methanol, DMF, and water display multiple broad turning points between 500

and 4000 G, Figure 7. The observed spectra are similar to those reported in the literature for other iron complexes with thiolate or chloride donors.(22, 50, 51) Despite the complexity of the spectra, the vast majority of the signal intensity (>99% of the spins) can be simulated as a single monomeric high-spin iron complex with trace quantities of a $g_{eff} \sim 4.3$ signal as described below.

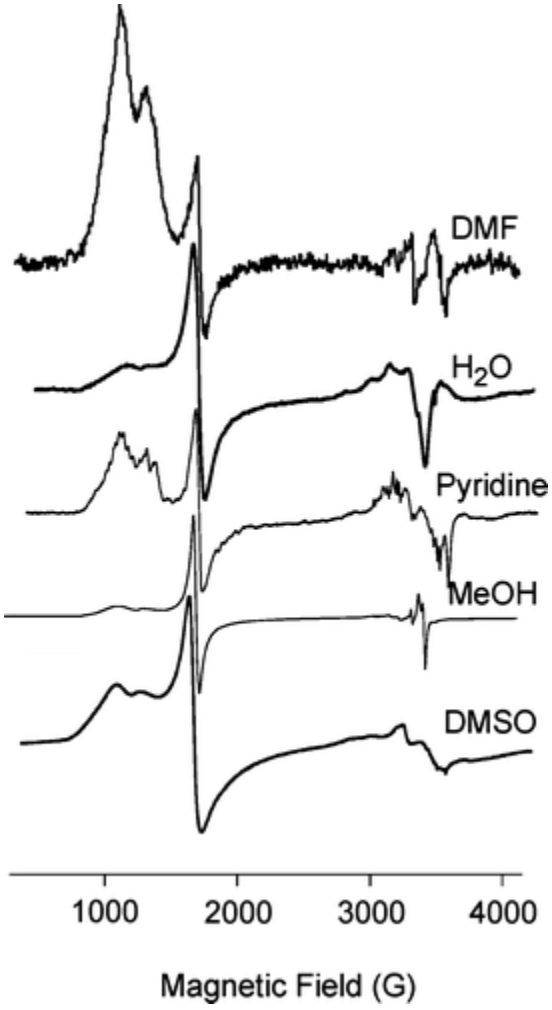

Figure 7. EPR spectra of **[LFe]OTf** in various solvents. All spectra recorded at 20 K except DMF (77 K).

The EPR signals shown in Figure 7 are similar to those reported for iron-catecholate complexes(52) in that the strain in *E* (here characterized as a strain in *E/D*) extended the envelope of *E/D* such that one of the "preferred" values of *E/D* was exhibited by some of the molecules. These preferred values give rise to apparently anomalously intense features in the EPR spectrum because of partial or total lack of orientation selection in the powder spectrum.(53) In the case of the catecholate species, the strains in *E* were sufficiently high that the spectra exhibited an intense component at $g_{eff} \sim 4.3$ because of a subpopulation with $E/D \sim 1/3$, although the mean value of *E/D* was as low as 0.120.

The strain-dependent appearance of the $g_{eff} \sim 4.3$ resonance can be appreciated by comparing the calculated spectra of Figure 8A and B, that have identical spin Hamiltonian parameters except for the strain in *E/D*. In the present case, the signals from **[LFe]OTf** exhibit low field lines that are split by only about 170 G (17 mT), compared to about 500 G (50 mT) for the catecholate complexes. Simulations (Figure 8B−E) indicate that the smaller splitting is due to a lower mean *E/D* value of 0.045. One of the consequences of this lower value for *E/D* is a change in the relative intensities of the two low field lines; g_x and g_y for the $m_S = 3/2$ Kramers'

doublet of S = 5/2 approach zero as E/D decreases, and the spectrum spans an increasingly wide field envelope, leading to a diminution of the intensity of the higher-field line of the pair (the g_z resonance of m_S = 3/2, at 1200 G [120 mT], $g_{eff} \sim 5.7$). As strains in E/D are introduced (Figure 8F–M), this feature appears to grow in intensity again. However, unlike the lowest field resonance of m_S = 1/2 at 1000 G (100 mT; $g_{eff} \sim 6.6$), the line at 1200 G does not become broadened at successively higher values of $\sigma E/D$. In addition, it shifts slightly to a resonance position corresponding to g_{eff} = 6.0 and assumes a typical g_x-g_y derivative shape. Thus the resonance observed is actually due to strain-dependent access of the preferred E/D value of zero, giving rise to an intense resonance due to the g_x and g_y transitions in m_S = 1/2. Only when very high E/D-strain is present is the $g_{eff} \sim 4.3$ line observed (Figure 8M). At such a high value of $\sigma E/D$, only the preferred resonances ($g_{eff} \sim 6$, $E/D \sim 0$ and $g_{eff} \sim 4.3$, $E/D \sim 1/3$) are resolved. As expected from the above assignment, the relative intensities of the $g_{eff} \sim 6$ and $g_{eff} \sim 4.3$ resonances change upon raising E/D, with the higher value of E/D favoring $g_{eff} \sim 4.3$.

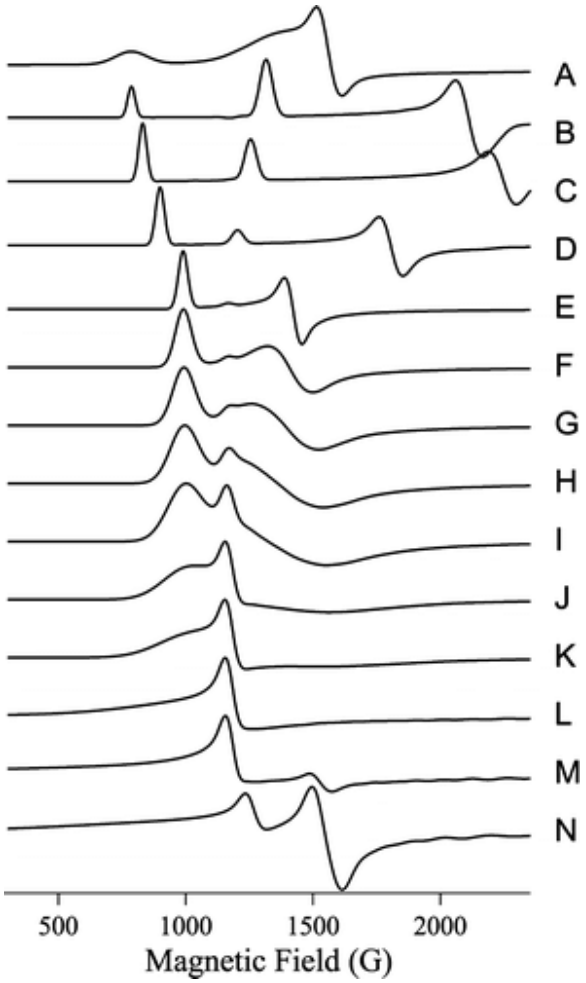

Figure 8. Calculated high-spin spectra. High-spin spectra were calculated assuming S = 5/2, g_{iso} = 1.995, and (A) D = 0.45 cm^{-1}, E/D = 0.165, $\sigma E/D$ = 0.08; (B) D = 0.45 cm^{-1}, E/D = 0.165, $\sigma E/D$ = 0; (C) D = 0.45 cm^{-1}, E/D = 0.125, $\sigma E/D$ = 0; (D) D = 0.45 cm^{-1}, E/D = 0.085, $\sigma E/D$ = 0; (E) D = 0.45 cm^{-1}, E/D = 0.045, $\sigma E/D$ = 0; (F) D = 0.45 cm^{-1}, E/D = 0.045, $\sigma E/D$ = 0.010; (G) D = 0.45 cm^{-1}, E/D = 0.045, $\sigma E/D$ = 0.015; (H) D = 0.45 cm^{-1}, E/D = 0.045, $\sigma E/D$ = 0.020; (I) D = 0.45 cm^{-1}, E/D = 0.045, $\sigma E/D$ = 0.025; (J) D = 0.45 cm^{-1}, E/D = 0.045, $\sigma E/D$ = 0.035; (K) D = 0.45 cm^{-1}, E/D = 0.045, $\sigma E/D$ = 0.045; (L) D = 0.45 cm^{-1}, E/D = 0.045, $\sigma E/D$ = 0.100; (M) D = 0.45 cm^{-1}, E/D = 0.045, $\sigma E/D$ = 0.320; (N) D = 0.45 cm^{-1}, E/D = 0.130, $\sigma E/D$ = 0.320.

From the simulations displayed in Figure 8, the high spin spectra of **[LFe]OTf** in H_2O, pyridine, DMSO, methanol, and DMF can be explained as containing contributions from a slightly rhombic (E/D = 0.045) S = 5/2 Fe(III)

species that exhibits strain in *E/D*, and an additional component that is responsible for the g_{eff} = 4.3 line. The strains in the slightly rhombic species result in a broadened resonance at $g_{eff} \sim 6.6$ due to the *E/D* envelope associated with the g_x transition in $m_S = 1/2$ and a resonance at $g_{eff} = 6.0$ due to the g_x and g_y transitions in a subpopulation with the preferred value of $E/D \sim 0$. As is also evident from the simulations, when *E/D* is sufficiently small to account for the resonance positions observed, and when σ*E/D* is sufficiently small that the $g_{eff} \sim 6.6$ resonance is resolved, there is no significant contribution to the spectrum from the $m_S = 3/2$ doublet, in contrast to the spectra of iron-catecholate complexes. The $g_{eff} = 4.3$ line must, therefore, arise from a separate Fe(III) species most likely because of complex degradation. The spectrum of **[LFe]OTf** in DMSO was simulated as such, Supporting Information, Figure S5, and integration of the simulations indicated that the slightly rhombic species that exhibit the $m_S = 1/2$ resonances accounted for 85% of the spins (note that much of the spectral intensity is at high field and is virtually undetectable in the derivative spectrum), and the $g_{eff} = 4.3$ line accounts for about 15% of the spins.

The EPR simulations for **[LFe]OTf** in DMSO reveal the majority of the spin density is attributable to the six-coordinate **[LFe-DMSO]OTf**. That the high-spin EPR signal indeed arises from solvent-bound species is evidenced by the spectra of **[LFe-pyridine]OTf**, in which pervasive superhyperfine coupling to nitrogen is present in the majority of the signal. Similar spectral characteristics displayed in σ-donor solvents are consistent with the formation of six-coordinate high-spin Fe(III) complexes. The spectrum of **[LFe-HOMe]OTf** also displays the sharp signal of **[LFe]**$^+$ (*g* = 2.04, 2.02, and 2.01) consistent with weak coordination. The predominance of the high spin complex despite the binding of strong σ-donors (e.g., DMSO, pyridine) suggests that π-affects are instrumental in determining the spin state of iron in these complexes.

Solvent Competition Studies

The unique ability of **[LFe]**$^+$ to bind both substrates (water and nitriles), as well as product (amide), provides the opportunity to directly probe binding preferences for iron in a nitrile hydratase model complex. The iron displays a preference for water over nitrile. Addition of nitriles to **[LFe-OH$_2$]**$^+$ at a pH of 3.0 shows no spectroscopically detectable changes in the UV−visible or EPR spectra. Addition of nitriles to **[(LFe)$_2$OH]**$^+$ at a pH of 6.1 (vide infra) also reveals no detectable changes. In contrast, addition of pH = 6.1 buffered H_2O (100 equiv of H_2O per Fe) to acetonitrile solutions of **[LFe]**$^+$in which the nitrile concentration exceeds the water concentration by three orders of magnitude results in significant spectroscopic changes. The charge transfer band in the UV−visible spectrum broadens and red shifts to 602 nm, and the EPR spectrum is silent consistent with formation of the dinuclear complex **[(LFe)$_2$OH]**$^+$ and no detectable quantities of **[LFe-NCMe]**$^+$.

Although the above experiments clearly demonstrate the affinity of iron for water over nitriles, this preference extends even when substoichiometric quantities of water are added to acetonitrile solutions of **[LFe]OTf**. Careful addition of 1 equiv of triflic acid to the μ-oxo complex **(LFe)$_2$O** in acetonitrile leads to a red shifting of the charge transfer band from 560 to 603 nm consistent with protonation of the oxo bridge yielding **[(LFe)$_2$OH]**$^+$, which is EPR silent (vide infra). Careful addition of a second equivalent of triflic acid protonates the bridging hydroxide generating 1 equiv of water for every 2 equiv of **[LFe]OTf**. Water coordination is confirmed spectroscopically by a shift in the low energy band from 603 to 628 nm, Supporting Information, Figure S7. The EPR spectrum of the reaction mixture, Supporting Information, Figure S8, reveals the expected iron-containing products **[LFe-OH$_2$]**$^+$ and **[LFe-NCMe]**$^+$ (in equilibrium with **[LFe]**$^+$).

The relative binding affinity of **[LFe]OTf** for amides as compared to nitrile and water was determined through additions of small amounts of DMF to solutions of **[LFe]OTf** in acetonitrile and pH = 5 buffered water, respectively. The UV−visible and EPR spectra of **[LFe-OH$_2$]**$^+$ in buffered aqueous solution remain unchanged upon addition of 10 equiv of DMF, denoting the preference for water over DMF. Addition of 10 equiv of DMF to acetonitrile solutions of **[LFe]OTf** is best monitored by EPR, since the UV−visible spectra of **[LFe]OTf** in the two

solvents is similar. The EPR shows no trace of the low spin signals of **[LFe-NCMe]**$^+$ or **[LFe]**$^+$. In fact, the spectrum is dominated by the high-spin signal previously observed for **[LFe-DMF]**$^+$. Overall, the competition studies reveal that **[LFe]OTf** prefers catalytically relevant ligands in the order H_2O > amide > nitrile.

Aqueous Chemistry

Given the strong preference for water coordination to **[LFe]OTf**, its aqueous chemistry was further explored. As outlined in Scheme 2, three discrete derivatives of **[LFe]OTf** are accessible as a function of pH. At pH < 5.0 (dilute triflic acid) **[LFe-OH_2]**$^+$ is present as a dark blue solution with bands at 315 and 613 nm. In addition to deprotonation events described below, the coordinate thiolates of **[LFe-OH_2]**$^+$ may be protonated but only at pH values lower than 3.00 at which point complex degradation occurs. Similar remarkable acid stability of an iron-thiolate has been previously reported for a NHase model complex with deprotonated amide donors in place of the amines found in **[LFe]OTf**.(10)

Scheme 2

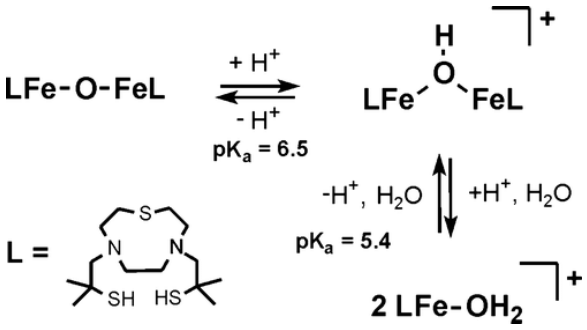

Titration of aqueous solutions of **[LFe-OH_2]**$^+$ with NaOH first yields the μ-OH complex **[$(LFe)_2OH$]**$^+$. Monitoring of the reaction by UV−visible spectroscopy reveals a blue shift of the low energy band from 613 to 603 nm. At pH = 6.10, the charge transfer band at 603 nm reaches its maximum intensity, and the solution develops an intense violet color. The violet solution is EPR silent suggesting a strong antiferromagnetic coupling of the two high-spin iron(III) centers. No intermediate is detectable by UV−visible spectroscopy suggesting the mononuclear **LFe-OH** rapidly proceeds to **[$(LFe)_2OH$]**$^+$ once generated. Continued titration of **[$(LFe)_2OH$]**$^+$ leads to a further blue shifting of the charge transfer band from 603 to 560 nm. The resulting burgundy colored solution is characteristic of the previously reported μ-oxo complex **$(LFe)_2O$**. Because of the poor water solubility of **$(LFe)_2O$**, reliable pK_a values could not be obtained. The titration was repeated in buffered 70:30 water/acetone mixtures yielding similar results, with the exception that **$(LFe)_2O$** did not precipitate, Supporting Information, Figure S6. From this data, the pK_a of the water bound complex **[LFe-OH_2]**$^+$ is estimated as 5.4 ± 0.1, while that of **[$(LFe)_2OH$]**$^+$ is 6.52 ± 0.05.

Trials for Catalytic Activity

The catalytic competency of **[LFe]OTf** toward the hydrolysis of nitriles was evaluated by addition of benzonitrile to room-temperature buffered aqueous solutions of **[LFe]OTf** at pH 6.10 and 3.03. At pH 6.10, **[$(LFe)_2OH$]**$^+$ is the dominant iron species in solution, while **[LFe-OH_2]**$^+$ is predominate at pH 3.03. The reaction mixtures were analyzed by gas chromatography for the presence of hydrolysis products benzamide and benzoic acid in organic extracts of the reaction mixture. No trace of hydrolysis products were detected under either set of conditions.

Conclusions and Relevance to Nitrile Hydratase

The complex **[LFe]OTf** has for the first time allowed direct competition studies to evaluate the relative binding affinities of water, nitriles, and amides in a nitrile hydratase model. The observed ligand binding affinity of H_2O > amide > nitrile reveals that water coordination is favored over nitrile binding. Additionally, the preference for

amides over nitriles further decreases the probability of a nitrile bound mechanism, since product release would also be problematic.

The only previously reported iron model complex of nitrile hydratase that coordinates nitriles, **[Fe^{III}(S$_2$^{Me2}N$_3$(Et,Pr))]$^+$**, cannot bind water because of ligand degradation in aqueous environments.(23) Our model binds nitriles with a similar affinity as **[Fe^{III}(S$_2$^{Me2}N$_3$(Et,Pr))]$^+$**, but it also binds water much more tightly. The coordination of water to **[LFe]OTf** is similar to that observed in the Mascharak model complex, **[Fe^{III}(PyPS)]$^-$**. However, in that case no nitrile binding was observed precluding a direct and definitive comparison with the **[Fe^{III}(S$_2$^{Me2}N$_3$(Et,Pr))]$^+$**model.(22) The Mascharak aquo complex is low-spin in contrast to our high-spin model suggesting that either spin state shows a strong affinity for water over nitriles. Our results bridge the prior studies and lend credence to a water-bound mechanism.

While both **[LFe]OTf** and **[Fe^{III}(PyPS)]$^-$** bind H_2O, the former is high-spin and the latter is low-spin.(22) The pK_a values reveal that the high-spin **[LFe-OH$_2$]$^+$** (5.4 ± 0.1) is almost ten times as acidic the low-spin **[Fe^{III}(PyPS)(H$_2$O)]$^-$** (6.3).(22) Recently we reported that oxygen sensitivity of iron-thiolates is likely spin-state dependent and question if similar effects may also influence the pK_a of coordinated water.(11) From a simple electrostatic approach, the relatively smaller ionic radius of low-spin iron(III) should *lower* the pK_a of bound-water more efficiently than high-spin iron(III). However, this approach ignores π-interactions between the metal center and water/hydroxide that have been shown to be important for low-spin, but not high-spin, Fe(III).(43) The π-interactions between the lone pair on HO^- and a filled/nearly filled "t_{2g}" orbital on low-spin Fe(III) would destabilize hydroxide coordination and *raise* the pK_a. Additionally, the π-interactions may promote the nucleophilic character of the coordinated HO^- similar to effects in metal–thiolates that yield nucleophilic sulfur.(54, 55) Overall, the low-spin state may modulate the pK_a while maintaining significant nucleophilic character. In contrast, the more acidic high-spin derivatives may lack a sufficiently nucleophilic hydroxide and even undergo further deprotonation to μ-oxo species in model complexes. Further studies to confirm these hypotheses are underway.

Supporting Information

Expanded experimental protocols, EPR and UV/visible spectra, and CV of **[LFe]OTf**, and EPR simulations of **[LFe-DMSO]OTf** in PDF format and crystallographic data in CIF format (CCDC 708538). This material is available free of charge via the Internet at http://pubs.acs.org.

Terms & Conditions

Acknowledgment

This work was supported by the National Science Foundation CAREER Award (CHE-0238137) with continued support by (CHE-0749965). M.S.M. thanks the Kentucky Research Challenge Trust Fund for upgrade of our X-ray facilities. EPR studies were supported in part by an NIH P41 grant (EB001980) to the National Biomedical EPR Center.

References

1 Grapperhaus, C. A., Patra, A. K., and Mashuta, M. S. Inorg. Chem.**2002** 41 1039 1041

2 Grapperhaus, C. A., Li, M., Patra, A. K., Poturovic, S., Kozlowski, P. M., Zgierski, M. Z., and Mashuta, M. S. Inorg. Chem.**2003** 42 4382 4388

3 Mascharak, P. K. Coord. Chem. Rev.**2002** 225 201 214

4 Kovacs, J. A. Chem. Rev.**2004** 104 825 848

5 Lugo-Mas, P., Dey, A., Xu, L., Davin, S. D., Benedict, J., Kaminsky, W., Hodgson, K. O., Hedman, B., Solomon, E. I., and Kovacs, J. A. J. Am. Chem. Soc.**2006** 128 11211 11221

6 Lee, C. M., Hsieh, C. H., Dutta, A., Lee, G. H., and Liaw, W. F. J. Am. Chem. Soc.**2003** 125 11492 11493

7 Kung, I., Schweitzer, D., Shearer, J., Taylor, W. D., Jackson, H. L., Lovell, S., and Kovacs, J. A. J. Am. Chem. Soc.**2000** 122 8299 8300

8 Harrop, T. C., and Mascharak, P. K. Acc. Chem. Res.**2004** 37 253 260

9 Galardon, E., Giorgi, M., and Artaud, I. Chem. Commun.**2004** 286 287

10 Artaud, I., Chatel, S., Chauvin, A. S., Bonnet, D., Kopf, M. A., and Leduc, P. Coord. Chem. Rev.**1999** 192 577 586

11 O'Toole, M. G., Kreso, M., Kozlowski, P. M., Mashuta, M. S., and Grapperhaus, C. A. J. Biol. Inorg. Chem.**2008**, *13*, 1219−1230.

12 Asano, Y., Tani, Y., and Yamada, H. Agr. Biol. Chem. Tokyo**1980** 44 2251 2252

13 Endo, I., Nakasako, M., Nagashima, S., Dohmae, N., Tsujimura, M., Takio, K., Odaka, M., Yohda, M., and Kamiya, N. J. Inorg. Biochem.**1999** 74 22 22

14 Endo, I., Odaka, M., and Yohda, M. Trends Biotechnol.**1999** 17 244 249

15 Kobayashi, M., and Shimizu, S. Nat. Biotechnol.**1998** 16 733 736

16 Nelson, M. J., Jin, H. Y., Turner, I. M., Grove, G., Scarrow, R. C., Brennan, B. A., and Que, L. J. Am. Chem. Soc.**1991** 113 7072 7073

17 Yamada, H., and Kobayashi, M. Biosci., Biotechnol., Biochem.**1996** 60 1391 1400

18 Shigehiro, S., Nakasako, M., Dohmae, N., Tsujimura, M., Tokoi, K., Odaka, M., Yohda, M., Kamiya, N., and Endo, I. Nat. Struct. Biol.**1998** 5 347 351

19 Hopmann, K. H., and Himo, F. Eur. J. Inorg. Chem.**2008** 1406 1412

20 Hopmann, K. H., Guo, J. D., and Himo, F. Inorg. Chem.**2007** 46 4850 4856

21 Greene, S. N., and Richards, N. G. J. Inorg. Chem.**2006** 45 17 36

22 Noveron, J. C., Olmstead, M. M., and Mascharak, P. K. J. Am. Chem. Soc.**2001** 123 3247 3259

23 Shearer, J., Jackson, H. L., Schweitzer, D., Rittenberg, D. K., Leavy, T. M., Kaminsky, W., Scarrow, R. C., and Kovacs, J. A. J. Am. Chem. Soc.**2002** 124 11417 11428

24 Armarego, W. L. F., and Perrin, D. D. Purification of Laboratory Chemicals; 4th ed.; Butterworth Heinimann: Oxford, 1996.

25 Gordon, A. J., and Ford, R. A. The Chemist's Companion: A Handbook of Practical Data, Techniques, and References, 1st ed.; Wiley: New York, 1973.

26 Shriver, D. F., and Drezdon, M. A. The Manipulation of Air-Sensitive Compounds, 2nd ed.; Wiley: New York, 1986.

27 Woodhouse, M. E., Lewis, F. D., and Marks, T. J. J. Am. Chem. Soc.**1982** 104 5586 5594

28 Evans, D. F. Proc. Chem. Soc.**1959** 115 2003 2005

29 Ellison, J. J., Nienstedt, A., Shoner, S. C., Barnhart, D., Cowen, J. A., and Kovacs, J. A. J. Am. Chem. Soc.**1998** 120 5691 5700

30 Albert, A., and Serjeant, E. P. Ionization Constants of Acids and Bases; Wiley: Methuen, NY, 1962.

31 Nilges, M. J. PhD.Thesis, University of Illinois, Urbana, 1979.

32 Hanson, G. R., Gates, K. E., Noble, C. J., Mitchell, A., Benson, S., Griffin, M., and Burrage, K. In EPR of Free Radicals in Solids: Trends in Methods and Applications; Shiotani, M., and Lund, A., Eds.; Kluwer Press: Dordrecht, The Netherlands, 2003.

33 SMART; Bruker Advanced X-ray Solutions, Inc.: Madison, WI, 2005.

34 SAINT; Bruker Advanced X-ray Solutions, Inc.: Madison, WI, 2003.

35 SADABS; University of Göttingen: Göttingen, Germany, 2003.
36 SHELXTL 6.14, Program Library for Structure Solution and Molecular graphics; Bruker Advanced X-ray Solutions, Inc.: Madison, WI, 2000.
37 Sheldrick, G. M. Acta Crystallogr., Sect. A Found. Crystallogr.**2008** A64 112 122
38 SHELXL-97, Program for the Refinement of Crystal Structures; University of Göttingen: Göttingen, Germany, 1997.
39 Farrugia, L. J. J. Appl. Crystallogr.**1997** 30 565
40 Dey, A., Jenney, F. E., Adams, M. W. W., Johnson, M. K., Hodgson, K. O., Hedman, B., and Solomon, E. I. J. Am. Chem. Soc.**2007** 129 12418 12431
41 Mosseri, S., Mialocq, J. C., Perly, B., and Hambright, P. J. Phys. Chem.**1991** 95 4659 4663
42 Evans, D. R., Mathur, R. S., Heerwegh, K., Reed, C. A., and Xie, Z. Angew. Chem., Int. Ed. Engl.**1997** 36 1335 1337
43 Evans, D. R., and Reed, R. A. J. Am. Chem. Soc.**2000** 122 4660 4667
44 Kennepohl, P., Neese, F., Schweitzer, D., Jackson, H. L., Kovacs, J. A., and Solomon, E. I. Inorg. Chem.**2005** 44 1826 1836
45 Noveron, J. C., Herradora, R., Olmstead, M. M., and Mascharak, P. K. Inorg. Chim. Acta**1999** 285 269 276
46 Griffith, J. S. Proc. R. Soc London, A**1956** 235 23 26
47 Taylor, C. P. S. Biochim. Biophys. Acta**1977** 491 137 149
48 Patra, A. K., Bill, E., Bothe, E., Chlopek, K., Neese, F., Weyhermuller, T., Stobie, K., Ward, M. D., McCleverty, J. A., and Wieghardt, K. Inorg. Chem.**2006** 45 7877 7890
49 Hopmann, K. H., Guo, J. D., and Himo, F. Inorg. Chem.**2007** 46 4850 4856
50 Rodriguez, M., Morenstern-Badarau; Cesario, M., Guilhem, J., Keita, B., and Nadjo, L. Inorg. Chem.**1996** 35 7804 7810
51 Strautmann, J. B. H., George, S. D., Bothe, E., Bill, E., Weyhermuller, T., Stammler, A., Bogge, H., and Glaser, T. Inorg. Chem.**2008** 47 6804 6824
52 Weisser, J. T., Nilges, M. J., Sever, M. J., and Wilker, J. J. Inorg. Chem.**2006** 45 7736 7747
53 Copik, A. J., Waterson, S., Swierczek, S. I., Bennett, B., and Holz, R. C. Inorg. Chem.**2005** 44 1160 1162
54 Mullins, C. S., Grapperhaus, C. A., and Kozlowski, P. M. J. Biol. Inorg. Chem.**2006** 11 617 625
55 Ashby, M. T., Enemark, J. H., and Lichtenberger, D. L. Inorg. Chem.**1988** 27 191 197